Tropical cyclone hazards and economic losses in coastal North Carolina

Jiahang He[1*], Jackson Parker[2], Brian Blanton[3], Christine Szpilka[4], Dahui Liu[5], Kendra Dresback[4], Randall Kolar[4], Brian Colle[2], Linda Nozick[6], and Ian Sue Wing[1]

[1]Boston University, Department of Earth & Environment, Boston, MA, USA
[2]Stony Brook University, School of Marine and Atmospheric Sciences, Stony Brook, NY, USA
[3]Renaissance Computing Institute, UNC Chapel Hill, Chapel Hill, NC, USA
[4]The University of Oklahoma, School of Civil Engineering and Environmental Science, Norman, OK, USA
[5]Donghua University, Glorious Sun School of Business and Management, Shanghai, People's Republic of China
[6]Cornell University, School of Civil and Environmental Engineering, Ithaca, NY, USA
[*]Corresponding author: email jhhe@bu.edu

ABSTRACT

Tropical cyclones threaten coastal regions through wind, storm surge, and inland flooding, yet risk assessments treat these hazards separately and rarely translate them into building-level losses. We pair 575,453 single-family homes ($443 billion) in eastern North Carolina with a 604-storm synthetic cyclone ensemble and physics-based models resolving wind, surge, and flood fields at 250-m resolution, translated to building-level damages. Separating each hazard's footprint from its severity reveals a systematic imbalance: wind reaches 62.9% of homes but is mild per event (5.1% mean loss ratio), whereas compound events are rare (0.19% of building–storm records) yet six to nine times more severe and contribute 9.4% of ensemble losses. Wind + flood compounds trace inland riverine corridors missing from surge-focused maps, and because they arise from spatial co-occurrence across the regional portfolio rather than additive damage at single structures, they undermine the diversification underpinning catastrophe insurance. The result is a protection gap: only 34.6% of homes carry wind and 10.2% flood coverage, over half of worst-case losses fall on the uninsured, and every home that cannot afford full coverage is compound-exposed—those most in need of protection are least likely to obtain it.

Introduction

vaidyanathan2016 vaidyanathan2016 vaidyanathan2016 vaidyanathan2016 Tropical cyclone (TC) vulnerability arises from the convergence of multiple compound hazards: strong winds, coastal storm surge, and extreme rainfall that generate both pluvial (surface) and fluvial (riverine) flooding. These hazards can intersect in space and time to generate compound events whose potential impacts exceed those produced by individual hazards in isolation[1]. For example, wind damage to a building envelope (loss of roof cover or wall failure) can facilitate water intrusion that an intact structure would otherwise resist, resulting in damage to the structure and its contents that are larger than the sum of losses from the two hazards acting independently. This example highlights the challenge of conceptualizing "extremes" from a societal, as opposed to a purely statistical, perspective.[2] This paper considers extremes as wind speeds and/or water inundation depths that are large enough to damage single family homes and incur monetary losses. We apply this definition to a region where combined TC-driven hazards are relatively common, the eastern coastal region of the US state of North Carolina (NC).[3]

The study area is an apposite test-bed for illustrating both the severity of TC exposure and the limits of single-hazard perspectives. Hurricane Florence (2018) delivered record-breaking precipitation in eastern NC, with some locations recording 35.93 inches (913 mm)—a 1-in-1000 year event[4]. The resulting catastrophic inland flooding accounted for much of the storm's human and economic toll, despite relatively modest wind speeds and limited surge penetration. Florence's rainfall was exacerbated by climate change[5], and the compound nature of its flooding could worsen in the future[6] due to increased rainfall rates and sea level rise.

Operational assessments and coastal flood risk tools have historically emphasized wind and surge inundation footprints, but rainfall-runoff processes are critical and freshwater flooding can generate losses inland that extend beyond FEMA-designated Special Flood Hazard Areas[7–10]. TC-caused extreme precipitation events have intensified in the Southeast U.S.[11], highlighting the need to quantify the relationships among wind, surge, and precipitation risks and inland losses.

Climatic change heightens the importance of this characterization. Sea-level rise and shifting TC climatology are projected to amplify surge inundation and increase near-storm rainfall rates[12,13]. TC climatology change dominates the amplification of joint rainfall-surge hazard for most of the U.S. coastline[14], increasing the likelihood of damaging flooding, both at the coast and far inland. Concurrent population expansion and property development have increased building exposure in surge-prone coastal zones and flood-vulnerable inland corridors, leading to a potential mismatch between where TC risk is measured and where it is experienced[15].

Application of risk-based insurance pricing without considering these phenomena threatens to concentrate affordability challenges in precisely those communities least able to bear the costs[16]. Actuarially sound pricing introduced by FEMA's Risk Rating 2.0 reform was associated with reductions in policy uptake, especially among low-income households[17]. Moreover, omission of inland flooding from hazard assessments can lead to misallocation of resources that over-emphasize coastal defenses while leaving inland communities under-protected[18].

The present study investigates these issues, advancing compound TC hazard characterization in North Carolina. Coupled hydrological-hydrodynamic modeling confirms the importance of riverine discharge as a boundary condition for coastal surge in low-gradient estuarine systems[19,20]. Simulation of historical landfalling TCs identified distinct compounding mechanisms along the Cape Fear Estuary and motivated the use of a synthetic TC ensemble approach to augment the relatively sparse historical record[7]. In a probabilistic compound flood assessment of >2,800 synthetic TCs, runoff processes accounted for more than 65% of the 1% annual flood extent, climate change increased compound flooding 12-25%, while sea-level rise shifted compound flood-affected zones inland[21]. However, analysis of wind and surge impacts on more than one million eastern NC buildings reveals a decline in monetary losses with social vulnerability because of the concentration of losses in high-value coastal property despite wind damage extending inland[22].

Key gaps are the lack of similar building-level analyses of inland flooding—the hazard that dominates total flood extent in both current and projected climates[6,21], and the limited translation of physical inundation into building-level monetary losses or insurance-relevant metrics among compound hazard assessments. To address these limitations we exploit the economic concepts of the extensive margin (hazards' geographic footprint and occurrence frequency) and the intensive margin (severity of losses conditional on damage occurring). This distinction matters for adaptation: extensive-margin metrics reveal where to target adaptation measures, while intensive-margin metrics identify what level of adaptation is appropriate. It also matters for property insurance risk pooling, where insurers collect premiums from many policyholders on the expectation that only a small number experience losses at any one time[18,23,24]. A single TC event can generate widespread wind and inundation losses that violate this spatial-independence assumption, with consequences for premiums, coverage uptake, and uninsured losses that have rarely been quantified[25,26].

Our approach is to develop an integrated, building-level framework to assess compound TC risk across both extensive and intensive margins. We combine 1.8 million georeferenced single-family houses from the 2022 National Structure Inventory[27,28] with 604 synthetic TC tracks and physics-based hazard models to generate joint wind + surge + flood intensity fields at 250m resolution.

The hazard modeling framework (Figure 1) uses synthetic TC tracks and intensities from the Tropical Cyclone Wind and Impact Simulation Environment (TCWiSE) tool[29] and wind fields computed by the Generalized Asymmetric Holland Model (GAHM)[30,31]. TC track parameters are used to drive the Precipitation-Climatology and Persistence (P-CLIPER) rainfall model[32] to generate spatial rainfall distributions for the Ensemble Framework for Flash Flood Forecasting (EF5)[33]. EF5 uses multiple water balance models and river routing schemes to determine the hydrological response in a region to rainfall events[34,35]. Finally, storm surge and waves are simulated with the ADvanced CIRCulation (ADCIRC) and Simulating WAves Nearshore (SWAN) models[36–38], forced by GAHM wind fields and riverine boundary conditions from EF5. (See Methods.)

[Insert Figure 1 Here]

We compute building-level losses using FEMA Hazus 7.0 damage functions[39], which translate wind and inundation exposures into fractional losses in the value of the structure and its contents for multiple residential building archetypes. Hazard exposures fall into eight mutually exclusive categories (no damage, wind-only, surge-only, flood-only, and four combinations of compound exposures) all based on damage-relevant thresholds: $>$55 mph (88.5 km/h) peak wind gusts and nonzero inundation depths. Damage functions are assigned to 575,453 single-family homes with a total replacement value of \$443Bn across the domain. We characterize the extensive margin using occurrence probabilities and exposure tabulations (population, building area, replacement value) by category, and the intensive margin using the conditional distributions of wind speed, storm surge, and flood depth and their associated building-level losses.

This analytical framework allows us to elucidate: (1) Where compound TC hazard footprints extend across eastern NC, and how their occurrence probabilities differ from those of individual hazards. (2) Conditional on damage, how compound events compare with single-hazard events in terms of average impact and contribution to ensemble loss totals? (3) How the low probability but high loss consequence of compound exposures results in a residual protection under voluntary insurance uptake, and which hazard categories drive tail uninsured losses.

We find that compound hazards extend inland from the coastline: footprints of wind + surge, wind + flood, and triple-hazard exposure and damage collectively span roughly 1,900 km^2, with wind + flood compound hazards following inland riverine corridors largely absent from traditional surge-focused risk maps. As non-zero losses increase from the median to the 99th percentile, compound footprints expand substantially, connecting coastal surge zones to inland flood corridors. Second, compound exposures are rare but damaging, accounting for only 0.2% of total building $\times$ storm event observations and $<$5% of nonzero damage observations, but 9% of total ensemble losses; when damage occurs, loss ratios (the area-averaged fractional loss of buildings' structure + content value) can be six to nine times higher than due to wind alone (32–47% versus 5%). Third, voluntary insurance uptake leaves a structural protection gap: only 35% of buildings purchase wind coverage and 10% purchase combined wind+flood coverage, resulting in worst-case uninsured losses of \$34B (60% of exposed value) under a wind-only policy and \$31B (54%) when insurers offer wind and flood policies. Compound hazard exposures account for 43-48% of these worst-case uninsured losses, which suggests that broadening the scope of hazards covered by insurance narrows the gap only modestly.

These results have implications for catastrophe insurance and resilience policy. Because compound exposure is concentrated at low occurrence probabilities, actuarial approaches that rely on historical claims frequency may under-represent multi-hazard risk, which points to a role for physically based, forward-looking assessments of the type presented here as inputs to programs such as FEMA's Risk Rating 2.0. The spatial co-occurrence of wind, surge, and flood losses across coastal and inland geographies within individual storms is also inconsistent with the independence assumptions used in risk pooling and can increase portfolio-level tail risk. At the same time, the inland riverine corridors identified as compound-risk zones—areas with conditionally severe flooding but limited prior hazard assessment—raise affordability considerations: risk-based pricing in these newly recognized areas may need to be paired with measures that address coverage gaps for households with limited capacity to self-insure. The extensive–intensive margin framework used here provides spatially explicit, building-level information that decision-makers can use to prioritize adaptation investments where compound exposure is concentrated and to calibrate protection levels to the conditional severity at each location.

Results

Extensive Margin Footprints of Compound Hazard Exposures

Across members of the 604-event ensemble, we compute the building-level probability of any of the eight combinations of the aforementioned exposures that are intense enough to cause damage, and are synonymous with the occurrence of monetary losses. These probabilities define the extensive margin: individual and compound hazard exposures in terms of (A) the fractions of population and assets in the study domain that experience damaging TC hazard impacts across the ensemble, (B) impacted homes' average probability of damage (each event impacts different subsets of properties), and (C) the size of impacted populations and assets at different quantiles of the probability distribution of nonzero losses (Table 1).

[Insert Figure 1 Here]

TC wind fields' broad geographic extent means that wind exposure and impacts dominate: ∼64% of homes, population and single family home value have a nonzero probability of sustaining wind losses (Table 1, Panel A). Surge and flood exposure footprints and associated impacts are limited to coastlines and rivers: ∼1.4% and ∼2.3% of homes/population/value, respectively. The latter circumscribe compound hazards' geographic footprints: wind + surge affect ∼2.6%, wind + flood ∼2.8%, coincident triple hazards just ∼0.3% of homes, population and value. Notwithstanding, absolute exposures can be substantial: homes with surge, flood, wind + surge, and wind + flood impacting \$14, \$21, \$24, and \$27 Bn in residential property value, respectively. Apart from wind, much of the study area's population and assets are unaffected by inundation and compound hazards. (The notable gap is pluvial flooding, which our modeling framework does not capture.) Despite these modest footprints, properties exposed to compound hazards make up an outside share of ensemble losses (Table 2).

For properties damaged by at least one event, Panel B reports the likelihood that damage occurs. Surge, which affects only 1.5% of all homes, has a loss probability of just 0.8% at the sample median, rising to 11% and 27% at the 95th and 99th percentiles of the distribution of affected homes in disproportionately exposed coastal communities. The flood damage distribution has a smaller median but a heavier tail, which corresponds inundation-prone properties along river banks that sustain flood losses in nearly every ensemble member. Compound hazard loss probabilities are much smaller by comparison, with wind + surge ranging from 1.2% (median) to 12.6% (P99), wind + flood ranging from 0.7% (median) to 7.5% (P99), and triple-hazard damage probability reaching only 3.1% (P99).

Panel C summarizes population and asset exposures at the loss distribution quantiles. Sample median exposure corresponds to 38,000 people and \$13 Bn in home value for wind + surge compound losses, and 61,000 people and \$14 billion for wind + flood. But the populations and assets exposed to the aforementioned tail risks are an order of magnitude smaller, <1,000 people and \$300 M for wind + surge, 1,400 people and \$300 M for wind + flood, and <1,000 people and \$40 M for triple-hazard exposure.

For most of the study area's people and property that suffer nonzero losses, exposure to damage is rare (Figure 2). Because wind is widespread across the domain, sizeable populations and amounts of residential real estate value have a 3-10% chance of experiencing damage from only wind. By comparison, significant but still smaller populations and asset bases have only a <2% chance of experiencing damage from only surge or flood (consistent with inundation hazards' localized character).

[Insert Figure 2 Here]

Exposure profiles for compound hazards lie between those for wind and inundation, more (less) skew than the former (latter), with majority of exposed population and assets experiencing losses with <5% probability. Consistent with Table 1, Panel B, two compound hazards are dominant, wind + surge and wind + flood. Wind + flood + surge is both very rare and limited in its potential impact, consistent with the fact that simultaneous exposure to the three hazards is spatially and temporally restricted: estuarine locations and a small subset of sufficiently severe landfalling storms. While direct comparison with the observational record is challenging, the rarity of these events is broadly consistent with the fact that out of 120 TCs affecting NC since 1980 only ∼15 storms approached triple-hazard severity, including hurricanes Floyd (1999), Isabel (2003), Matthew (2016), and Florence (2018).

These results suggest that actuarial calculations that rely on the frequency of historical insurance loss claims are likely to systematically underestimate compound hazard risk at locations where per-storm occurrence probabilities fall below 5%—exactly where the largest compound exposures are concentrated. Our physically based probabilistic framework captures these low-probability, high-consequence events that observational records alone cannot resolve.

Intensive Margin Exposure and Loss Severity

We now turn to the intensive margin, considering how exposure, property damage and associated monetary losses change with hazard severity. Figure 3 shows conditional distributions of population, asset value, and loss functions of hazard intensity for each individual hazard type, filtering the large mass of sub-tropical storm wind speeds and zero inundation-depth observations. Wind speed is reported in mph (1 mph $\approx$ 0.447 m s^{-1}) and inundation depth in ft (1 ft $\approx$ 0.305 m), following the Hazus damage functions (see Methods).

[Insert Figure 3 Here]

The first two rows of Figure 3 demonstrate how population and asset exposures decline as hazard intensity increases. Wind exposure (left column) decreases steadily from peak values at tropical-storm-force speeds ∼ 40-60 mph, with the exposed population falling from about 400,000 to near zero as wind speeds approach 250 mph. Surge exposure (center) is concentrated at shallow depths (1-3 ft), declining sharply beyond 5 ft. Flood exposure (right) similarly peaks at shallow depths (1-3 ft) before tapering, though with a longer tail extending beyond 20 ft in extreme events.

The third row reveals the competing effects of shrinking hazard footprints and intensifying per-structure damage. Despite the rapid decline in exposed population and assets at higher intensities, wind losses peak not at the lowest speeds but at moderate-to-high speeds (80-150 mph), where the marginal increase in the damage rate per structure is sufficient to offset the declining number of exposed buildings. The median wind loss reaches approximately \$ 20-40 billion at these intermediate intensities, with the 95th-percentile envelope extending to \$ 50-60 billion. For surge, the loss distribution is more heavily skewed: losses peak at relatively shallow depths (2-4 ft) because these depths coincide with the largest exposed populations. Flood losses are more broadly distributed across depths: alongside the shallow-depth peak, the median loss profile exhibits secondary peaks near 7 ft and 20 ft, where deep riverine inundation intersects exposed communities along major river corridors. In both cases, the long-tailed character of the ensemble – visible in the wide 95% confidence bands – indicates that individual storms can produce substantial losses at much greater depths.

Intensive Margin: Compound Hazard Interactions

The individual hazard distributions in Figure 3 highlight that each intensity bin is itself a distribution across storms—one that, for compound events, must be understood in two hazard dimensions simultaneously. Figure 4 presents the joint distributions of wind speed and inundation depth for the two compound combinations that the extensive margin identifies as most consequential: wind + surge and wind + flood.

[Insert Figure 4 Here]

For wind +surge compounds (Fig. 4b), population and asset exposure at the median storm level are concentrated where moderate wind speeds (50-100 mph) coincide with shallow-to-moderate surge depths (1-5 ft), characteristic of the broad coastal zone affected by typical storms. As non-zero loss increases toward the 95th and 99th percentiles, the exposed population shifts toward higher wind speeds (100-200 mph) and deeper surge (3-10 ft), with the densest exposure cells exceeding 600,000 people at extreme combinations. The loss panels (bottom row) reveal that compound wind + surge losses are concentrated at high wind speeds (100-200 mph) and moderate surge depths (2-8 ft), with 99th-percentile losses reaching \$5-7.5 billion in the most damaging intensity bins. Notably, losses intensify more steeply with wind speed than with surge depth, suggesting that wind damage amplifies surge losses more than the reverse–consistent with the physical mechanism of wind-driven structural compromise preceding water intrusion. More broadly, the compactness of the wind + surge joint distribution at high wind / moderate surge intensities reflects synchronous coastal forcing: surge requires sustained onshore winds, so wind and surge maxima coincide in time and space at landfall.

For wind + flood compounds (Fig. 4a), the joint intensity space is more dispersed. At the median storm level, the exposed population is spread over a wide range of wind speeds (50-200 mph) and flood depths (0-15 ft), reflecting the geographic diversity of inland riverine corridors affected by TC rainfall. As severity increases, population and asset exposure is concentrated at moderate-to-high wind speeds (80-150 mph), with the densest cells—exceeding 10,000-12,500 people—at shallow-to-moderate flood depths (0-8 ft). Compound wind + flood losses at the 99th percentile reach \$200-300 million in the most damaging bins, an order of magnitude smaller than wind + surge losses, consistent with the more localized nature of riverine flooding relative to coastal surge. The dispersion of the wind + flood joint distribution, by contrast, reflects the spatial and temporal decoupling of inland riverine response from peak wind: TC-driven rainfall routes through river networks for hours to days after landfall, producing inundation in inland corridors not directly under the strongest winds.

The contrast between the two panels underscores a key asymmetry: wind + surge compounds are driven by the broad spatial coincidence of wind fields and coastal inundation during direct landfalls, producing concentrated, high-value losses along the coast. Wind + flood compounds, by contrast, arise from the interaction of wind damage with rainfall-driven riverine flooding along inland corridors, affecting fewer assets per event but spanning a wider and less predictable geographic range. Both compound types produce losses that increase nonlinearly with storm severity, but the physical mechanisms and the appropriate adaptation responses differ fundamentally.

These physical distinctions are borne out by the correlation structure of co-occurring perils (Table S9). Across building–storm records in which both perils cause damage, wind and surge intensities are weakly but positively correlated (Spearman $\rho = 0.28$), consistent with their synchronous coastal forcing, whereas wind + flood and flood + surge intensities are essentially uncorrelated ($\rho = -0.01$ and 0.00)—reflecting the temporal decoupling of rainfall-driven riverine response from peak wind and surge. The corresponding dollar losses, by contrast, are positively correlated in every pair (Pearson $r = 0.30$, 0.52, and 0.72 for wind + flood, wind + surge, and flood + surge), because co-located structures share exposure to the same storm's severity: where two perils strike together, a more damaging event in one tends to accompany a more damaging event in the other, concentrating rather than diversifying loss.

We do not present a separate bivariate figure for flood + surge compounds. As Table 1 demonstrates, flood + surge co-occurrence without wind affects only 0.08% of homes, with \$740 million in exposed value—more than an order of magnitude smaller than the other compound categories—because the near-ubiquity of TC-force winds during surge-producing storms means that the vast majority of flood + surge events also include wind damage.

Spatial Architecture of Compound Loss

The extensive and intensive margin analyses converge in the tricolor composition maps (Fig. 5), which display the proportional contribution of each hazard type to total building losses at the census-block level across three nonzero-loss quantiles.

[Insert Figure 5 Here]

At the median storm level (Fig. 5 a), wind and flood losses each account for $1.4 billion in aggregate losses: wind (cyan) dominates the domain's spatial extent, while flood losses (magenta) trace riverine corridors extending well inland. Surge contributes $0.5 billion, concentrated along the immediate coastline and barrier islands. Compound hazard footprints are minimal at this severity level: wind + surge and wind + flood contribute only $0.1 billion and $0.2 billion, respectively, while surge-flood and triple-hazard losses are negligible. The sparse outlined blocks along the coast and estuaries indicate the limited spatial extent of compound damage under typical storm conditions.

As non-zero loss increases toward the 95th percentile (Fig. 5 b), both single- and compound-hazard losses intensify dramatically. Wind losses rise to $335.0 billion, reflecting the broad spatial coverage of wind fields across eastern North Carolina. Compound footprints also expand markedly: wind + surge losses reach $14.3 billion, extending along tidal waterways and barrier island systems; wind + flood compounds contribute $12.4 billion, with purple markers tracing riverine corridors across the Coastal Plain. For the first time, triple-hazard losses become appreciable at $1.6 billion, appearing at low-lying confluences of coastal and fluvial systems. Surge-flood compounds without wind remain small ($0.3 billion), consistent with the near-ubiquity of damaging winds during surge-producing storms.

At the 99th percentile (Fig. 5c), compound losses grow further still: wind + surge reaches $32.1 billion and wind + flood $22.1 billion. The wind + flood compound footprint (purple markers inland) now forms a visually distinct network of riverine corridors extending from the coast through the Coastal Plain into the Piedmont–a geography largely absent from traditional surge-focused risk maps. Wind losses dominate the aggregate at $648.6 billion, yet the compound categories collectively account for over $57 billion, underscoring that compound events can generate economically consequential losses that grow nonlinearly with storm severity even though they are spatially limited.

Aggregate Loss Contribution and Conditional Severity

When compound hazards do materialize, they produce substantially more severe damage than single-hazard events. Mean conditional losses for compound events range from $275,465 (wind + flood) to $338,329 (triple-hazard), compared to $54,052 for wind alone–a five- to sixfold increase (Table 2). Conditional loss ratios for compound events average 31.5% (wind + surge), 35.1% (wind + flood), and 46.7% (triple-hazard), versus 5.1% for wind-only damage. The severity differential is even more pronounced in the tail: 95th-percentile losses for triple-hazard events reach $1.15 million per building with a loss ratio of 87.4%, indicating near-total structural damage.

[Insert Figure 2 Here]

Although they comprise only 0.19% of all building-storm observations, compound events contribute $422.7 billion in aggregate losses, which is 9.4% of the $4,508 billion ensemble total (Table S4). Wind + surge compounds alone account for $244.0 billion (5.4%), making them the single largest compound loss contributor. Wind + flood compounds add $166.5 billion (3.7%), while triple-hazard events contribute $11.0 billion (0.2%). By contrast, wind-only events generate 81.2% of total losses across 9.0% of observations, confirming wind as the dominant loss driver in absolute terms but underscoring that compound events are disproportionately costly per occurrence.

However, at the individual building level, an important structural characteristic is that in 99.8% of building-storm pairs, the maximum single-hazard loss equals the total loss across all hazards (Table S5). The total sum of individual hazard losses across the ensemble ($4,612 billion) exceeds the maximum-based total ($4,508 billion) by only 2.3%. This pattern indicates that compound hazards amplify regional losses primarily through spatial co-occurrence rather than through additive damage from multiple mechanisms at the same structure. In other words, different buildings within the same storm experience damage from different dominant hazard types. The implication for loss modeling is that the spatial correlation of hazard footprints, not the within-building superposition of damage, is the primary channel through which compound events elevate portfolio-level risk.

Aggregating across the full ensemble, 91.3% of structures (525,170 buildings; $406 billion) experience only single-hazard damage throughout all 604 storms, while 8.3% encounter compound events in at least one storm (Table S1). Buildings classified as compound-prone face substantially higher mean occurrence probabilities (27.6 % for two-hazard and 33.6 % for three-hazard buildings) compared with 13.5 % for exclusively single-hazard structures. This recurrence pattern indicates that compound-prone locations are not merely unlucky in isolated storms but are systematically positioned at physical intersections of multiple hazard mechanisms, experiencing repeated multi-hazard events across the ensemble.

Insurance Market Outcomes Under Compound Hazard

To quantify how compound TC hazard translates into insurance market outcomes, we apply the Cournot-Nash insurance model (see Methods) to the 196,619 single-family residential structures located within the coastal pricing footprint of eastern North Carolina—the area in which insurers actively price bundled wind and flood coverage and for which the hazard ensemble provides joint wind, surge, and flood loss estimates. This narrowing from the 575,453 residential structures used in the physical-loss analysis reflects the geographic scope of the priced coastal insurance market rather than a sampling decision. Within the synthetic ensemble, this coastal sample captures the bulk of surge-involved compound exposure statewide: 70.1% of all buildings that ever experience a wind + surge event (80,566 of 114,951) and 62.7% of those exposed to the wind + surge + flood triple (8,966 of 14,294). The remainder of the statewide compound-exposed inventory consists predominantly of inland wind–rainfall–flood combinations that lie outside the priced coastal market; across all compound categories combined, the sample covers 93,893 of 226,947 statewide compound-exposed buildings (41.4%). The model partitions these buildings into nine pricing zones based on expected loss per dollar of insured value, with equilibrium prices ranging from \$1.35 to \$4.21 per dollar of expected loss (Figure 6; Table S8).

[Insert Figure 6 Here]

Across the full study area, 34.6% of buildings (67,979) purchase wind insurance, but only 10.2% (20,149) purchase flood insurance. Every flood-insured building also carries wind coverage; no building purchases flood insurance alone. This asymmetry reflects the demand-side structure of the model: wind losses are spatially pervasive and generate sufficient expected utility loss to motivate insurance purchase across a broad range of risk attitudes, whereas flood and surge losses are spatially concentrated and affect fewer homeowners above the threshold at which coverage becomes utility-improving.

The expected-loss protection gap is most acute among the 94,069 buildings exposed to compound hazards—those facing positive expected losses from both wind and at least one water-based peril, and 47.8% of the priced sample. Only 21.4% of these compound-exposed buildings carry flood coverage; the remaining 78.6% are entirely uninsured against water perils. As a result, 80.9% of expected flood and surge losses across compound-exposed buildings fall on uninsured homeowners. Among compound-exposed buildings, flood uptake does not decline monotonically with price: it ranges from 18.4% in the zone that contains the largest number of such buildings (\$2.72 per dollar of loss) to 46.7% in a moderately priced zone (\$2.40), while the least expensive substantial zone (\$2.00) reaches only 27.5%. Pricing is therefore not the sole determinant of coverage–local risk characteristics and the heterogeneity of risk attitudes also shape demand.

Beyond the expected-loss gap, the aggregate worst-case protection gap depends on which policy the insurer offers. We compute worst-case uninsured losses under two insurer-offered scenarios (a wind-only policy and a combined wind + flood policy) by identifying the single storm from the 604-storm ensemble that produces the largest uninsured loss under that scenario's coverage rules, and attributing that loss to the hazard category of the driving storm (Table 3). Under a Wind-only offering, aggregate worst-case uninsured losses total \$34.1,B, equivalent to 59.8% of total building-plus-contents value across the sample (\$57.0,B). Under a Wind+Flood offering they fall to \$30.9,B (54.1% of exposed value). Because every household that buys flood coverage also retains wind coverage, the broader policy can only reduce the uninsured burden—but the reduction is modest, from 59.8% to 54.1% of exposed value, because only 10.2% of buildings elect flood coverage, leaving the remaining 89.8% exposed to uninsured water losses. The wind-only policy already reimburses the dominant peril for the 34.6% of buildings that take it up, so most of the achievable reduction in the aggregate gap is captured by wind coverage alone.

Decomposing these worst-case uninsured losses by hazard category reveals that compound-hazard storms account for a first-order share of the burden under both policy scenarios. Under the Wind-only policy, compound events (wind+surge, wind+flood, surge+flood, and wind+surge+flood) drive \$16.4,B, or 48.1%, of worst-case uninsured losses; individual hazards account for the remaining 51.9% (\$17.7,B). Under the Wind+Flood policy, compound events drive \$13.3,B (43.0%) of worst-case uninsured losses, with individual hazards accounting for 57.0% (\$17.6,B). The compound burden falls modestly in absolute terms across the two designs (\$16.4,B vs. \$13.3,B), because the flood policy—which indemnifies surge as well as inland flood—absorbs part of the compound water loss for the minority who buy it, while individual-hazard losses hold essentially flat (\$17.7,B vs. \$17.6,B) since a wind+flood buyer retains wind coverage. In both scenarios, the wind+surge combination is the single largest compound contributor (\$12.7,B under Wind-only; \$10.6,B under Wind+Flood), consistent with the spatial and temporal coincidence of hurricane wind fields and coastal surge inundation. These results indicate that compound events are not a second-order correction but a structural component of worst-case uninsured exposure, and that policy design alone—expanding the perils an insurer covers—does not close the protection gap so long as voluntary uptake of flood coverage remains low.

Equilibrium premiums substantially exceed expected losses at every pricing zone. The mean annual premium for wind-only policyholders is \$4,243, approximately 2.7 times their mean expected wind loss (\$1,572). For buildings carrying both wind and flood coverage, mean combined premiums total \$6,248, roughly 2.6 times the mean expected compound loss (\$2,432). These loading factors, which cover reinsurance costs, the solvency constraint, and insurer profit margins, increase monotonically with zone risk: from a premium-to-loss ratio of 1.9 in the lowest-priced zone to 4.1 in the highest-priced zone. The escalation of loading factors with risk level implies that actuarially sound pricing places the heaviest relative burden on the most hazard-exposed properties, precisely those for which the consequences of non-insurance are most severe.

[Insert Figure 3 Here]

All of the outcomes above are those of a market operating under an affordability constraint that caps each household's premium at 5% of its home value. Relative to an otherwise identical equilibrium solved without that cap, the constraint lowers equilibrium prices in seven of the eight pricing zones and raises coverage penetration in six of them—region-wide, from 32.1% to 34.6% of the priced sample—while compressing insurer margins in the highest-risk zones and reducing regional profit by roughly 38%, from \$42.8 M to \$26.6 M (Table S8). The cap therefore shifts the market in the direction policymakers intend. Yet it does not close the gap where it matters most: full wind-plus-flood coverage remains unaffordable for 4,790 homes whose offered premium still exceeds 5% of value even at the capped prices, and every one of these homes is compound-exposed—facing positive expected losses from both wind and at least one water peril (Fig. S10). Affordability failure is therefore not a wind-only or a water-only phenomenon but a compound-hazard one, concentrated in the coastal and estuarine zones where perils converge. Premium caps alone thus do not protect the households most exposed to multiple hazards.

Discussion

The extensive-intensive margin framework reveals a fundamental imbalance in TC risk that aggregated metrics obscure. Wind exposure is geographically extensive but produces low per-event severity: it dominates the spatial footprint in the simulated scenarios, yet generates mean loss ratios of only 5.1 %. Inland flooding shows a different pattern. It is geographically limited but severe per event, with mean loss ratios seven times higher than wind. This imbalance means that different adaptation instruments should be implemented for different locations. Areas facing frequent but mild wind exposure benefit from cost-effective building envelope improvements, whereas inland communities experiencing rare but severe compound flooding require more substantial interventions such as elevation, flood-proofing, or managed retreat. The extensive margin identifies where to invest; the intensive margin identifies how much protection is needed. This is a separation that echoes prior U.S. flood risk findings showing that the geography of exposure and the conditional distribution of damages require distinct policy responses[15,21,22].

Notably, buildings in compound-prone locations are not experiencing isolated multi-hazard events. They face recurrent exposure across the ensemble, with occurrence probabilities two to two-and-a-half times higher than single-hazard structures. This recurrence concentrates risk in identifiable geographic locations where targeted adaptation investments would yield the greatest reduction in expected losses.

A central interpretive finding is that compound hazards amplify regional losses through spatial co-occurrence. Different buildings within the same storm sustain damage from different hazard types rather than through additive damage at individual structures. This distinction matters for insurance because it undermines the geographic diversification assumptions that underpin catastrophe portfolio theory[18,23]. When a TC simultaneously causes coastal surge and inland flood losses, the entire regional portfolio suffers correlated losses, reducing the risk-spreading benefit of geographic diversification[24].

The concentration of compound exposure in low-frequency, high severity events further complicates actuarial practice. Historical claims data – typically spanning a few decades – cannot reliably estimate loss distribution for events with multi-century return periods. Forward-looking, physics-based synthetic storm ensembles are essential inputs for programs such as FEMA's Risk Rating 2.0[17,25]. At the same time, assessments like ours that have recently identified inland communities as compound-risk zones raise affordability concerns: actuarially sound pricing must be paired with mechanisms to prevent coverage gaps among populations least able to self-insure[26,40].

Our analysis extends prior compound hazard work from physical characterization to building-level economic impact quantification. Gori et al. (2020) identified compounding mechanisms along the Cape Fear Estuary using historical TCs[7], while we find that these patterns generalize across Eastern Carolina region at building resolution. Grimley et al. showed that the 1% annual flood hazard grows by 36% under high emissions, with compound flooding nearly doubling from 12% to 25%[21]; our building-level loss translation demonstrates that such hazard changes map to disproportionate economic impacts. Liu et al. assessed wind and surge losses across NC structures[22]; we complete the hazard triad by incorporating inland flooding, expanding the geography of assessed risk into inland corridors where more socially vulnerable populations are concentrated.

Our compound exposure estimate (7.6% of building value) appears lower than Ali et al.'s finding that ∼80% of historical coastal flood events involve compound drivers[41]. This reflects a methodological distinction: we classify buildings by whether co-occurring hazards each produce damage, not merely by the co-occurring hazards of physical drivers. The 80% event-level compound rate is consistent with our observation that compound damage, though rare at individual building level, occurs across the regional portfolio in a majority of storms.

Three limitations should be noted. First, the hazard chain has two scope limitations. Our rainfall fields are produced by P-CLIPER, which uses parametric, intensity-class-driven equations to generate symmetric rain fields around the storm center. This formulation cannot represent interaction with synoptic-scale weather fronts and the influence of pre-existing soil moisture on flood response—both of which played central roles in Hurricane Helene in 2024, in which a stationary front and saturated Appalachian soils produced totals far exceeding what TC intensity alone would predict. Such storms are therefore not captured regardless of the surge-screening threshold; looser cutoffs (0.25 m) admit Gulf-landfall tracks but most produce near-zero modeled rainfall over the Carolinas, confirming the constraint is rainfall physics, not track inclusion. Inland inundation is derived from EF5/CREST stream discharges via the HAND method, which captures fluvial flow but omits pluvial (surface-pooling) processes, so inland flood exposure represents a lower bound. Beyond scope, the fluvial chain itself carries structural and parameter uncertainty: kinematic-wave routing and stage–discharge relationships are extrapolated from sparse USGS gauge records, reservoir operations on the regulated Neuse, upper Cape Fear, and Roanoke rivers are not represented, and hydrologic calibration is limited to a single domain-wide routing adjustment. Channel misalignment in the hydrologically conditioned DEM also routes main-stem flow into secondary channels along a small number of flagged reaches—most notably the Tar River near Grimesland and the Brunswick River at Leland—where local inundation depths should be treated as suspect, although the resulting loss ratios fall within the range observed elsewhere in the domain (see Supplementary Information for implementation details, known problem areas, and ongoing model revisions). Second, the building-level damage model is conservative in two ways: our maximum-damage aggregation rule avoids double-counting but does not capture interaction effects such as wind-driven water intrusion amplifying surge damage (a bounded-additive sensitivity is reported in Methods); and the Hazus depth–damage and wind-fragility curves are central estimates whose published uncertainty bands are not propagated, so per-storm losses carry damage-function uncertainty not reflected in the ensemble spread. Third, the analysis uses present-day building stock and climatology—under future warming, compound flooding may nearly double[14,21], so our estimates likely understate future risk—and the inventory is restricted to single-family residential structures; extending coverage to commercial, multi-family, and critical infrastructure is the focus of ongoing work.

Conclusion

This study presents the first building-level assessment of compound TC risk that jointly quantifies wind, storm surge, and inland flooding losses across a large synthetic storm ensemble. By integrating 575,453 geo-referenced residential structures with 604 synthetic TCs and physics-based hazard models, and translating physical intensities into monetary losses via Hazus damage functions, we bridge the gap between compound flood hazard science and operational risk assessment.

Our extensive-intensive margin framework reveals that compound TC risk is both more geographically widespread and more conditionally severe than single-hazard assessments suggest. Wind + flood compound footprints extend into inland riverine corridors largely absent from traditional surge-focused risk maps, while severe fluvial flooding, though rare, produces conditional loss ratios seven times higher than wind. These findings reframe where adaptation resources should be directed and what level of protection is needed. Critically, compound hazards amplify regional portfolio losses through spatial co-occurrence across coastal and inland geographies, challenging the diversification assumptions that underpin catastrophe insurance pricing.

The framework demonstrated here is readily transferable to other TC-prone regions and provides the spatially granular, building-level risk information that programs such as FEMA's Risk Rating 2.0 increasingly require. Future work should incorporate climate change projections and sea-level rise, under which compound flooding contributions may nearly double[21]—as well as pluvial flooding processes, broader building types, and damage models that capture multi-hazard interaction effects. Pairing actuarially informed risk pricing with affordability safeguards will be essential to ensure that newly identified inland communities in compound-risk zones are not priced out of coverage.

Methods

Building Inventory

We employ the National Structure Inventory (NSI) version 2.0, a geo-referenced database of building-level attributes covering the continental United States[27]. For our study area in eastern North Carolina, we extract 1.8 million geo-referenced single-family houses from the NSI. Each record includes latitude–longitude coordinates (approximately 1-m horizontal precision) and core structural attributes needed for vulnerability mapping, including Hazus occupancy classification, number of stories, foundation type, primary construction material, year built, and replacement-value estimates for structure and contents.

We use NSI replacement values as our baseline exposure measure. To enable efficient hazard–inventory matching, we rasterize NSI point locations to a 250-m grid by rounding coordinates to the nearest 0.0025 decimal degrees (approximately 250 m at 35°N latitude). This resolution aligns with hazard model outputs and preserves within-block heterogeneity while reducing computational burden. Census block assignments use 2020 boundaries, updated from NSI's original 2010 geography via NHGIS block-to-block crosswalks with area-weighted allocations for split blocks[42]. The resulting analysis table includes building ID, 250-m grid cell, 2020 census block FIPS, occupancy type, construction attributes, and structure/contents replacement values.

Hazard Modeling

Overview

The hazard modeling framework, adapted and extended from previous work[19,20], generates a statistically robust dataset of TC-related hazards for North Carolina by integrating statistical and numerical models to simulate 1,000 years of combined wind, rainfall-induced fluvial flooding, and coastal storm surge. The model workflow (Figure 1) proceeds as follows.

Synthetic TC tracks are generated using the TCWiSE statistical track model[29]. Given a historical occurrence rate of approximately 10.8 tropical cyclones per year in the North Atlantic basin, the 1,000-year simulation produces more than 10,000 events. This set is subsequently reduced to 604 events that generate more than 0.5 m of surge along the North Carolina coast, identified using a fast, coarse-resolution ADCIRC screening grid. For this reduced population, the full high-resolution model suite computes the integrated hazard for each event. TCWiSE track parameters drive the parametric rainfall model P-CLIPER[32], whose output forces the EF5 hydrologic modeling system[33] to compute stream discharges and fluvial inundation extents. ADCIRC then computes coastal storm surge on a high-resolution unstructured grid. The integrated framework yields inundation extent, tropical cyclone-force wind exposure, and riverine flooding for each synthetic event. Detailed descriptions of each model component are provided in the following sections.

Synthetic Tropical Cyclone Tracks

TCWiSE uses a Monte Carlo framework to generate plausible TC tracks and parameters from statistical distributions of the historical TC record. TCWiSE first ingests user-specified parameters and International Best Track Archive for Climate Stewardship (IBTrACS) data[43,44] to calculate genesis and lysis probabilities for 5°×5° cells throughout the basin of interest. Kernel density estimation (KDE) is then applied to construct change functions for three key variables—forward speed, heading, and maximum sustained wind speed—for each grid cell, and these distributions are stored for use by the empirical track model (ETM). The ETM is a Markov model that computes location, heading, forward speed, and maximum sustained wind speed at each time step by randomly sampling the pre-generated KDE distributions conditioned on current values and grid cell location. At each time step, TCWiSE evaluates termination criteria based on lysis probabilities and wind speed and sea surface temperature thresholds. A final validation step removes tracks that never reach tropical storm strength.

As input for TCWiSE, we use observed TC data from IBTrACS covering the period 1980–2024 to minimize pre-satellite era biases[45] and sea surface temperature from the NOAA High-resolution Blended Analysis of Daily SST dataset[46] averaged into monthly means. Although TCWiSE'S KDE partially captures TC weakening over land, biases persist when compared to the historical record[29,47]. Therefore, we use an empirical and widely used post-landfall exponential decay model[48] with a decay parameter of 0.044[49] to model overland intensity weakening. All remaining parameters follow the default settings[29].

Several post-processing steps prepare the synthetic tracks for input into subsequent hazard models. Because TCWiSE does not model central pressure, we compute the pressure deficit (storm center to outermost closed isobar) using a 2-D quadratic regression of latitude and maximum wind speed derived from IBTrACS data spanning 2000 to present. Wind and pressure fields are then computed using the Generalized Asymmetric Holland Model (GAHM)[31] implemented within ADCIRC. The GAHM improves upon the original Holland model[30,50] by relaxing the cyclostrophic balance assumption at the radius of maximum winds and adopting a composite storm wind method. It accepts synthetic tracks in the Automated Tropical Cyclone Forecasting (ATCF) format and computes 10-m winds and sea level pressure either on a user-specified grid or directly on the ADCIRC grid.

Precipitation

The P-CLIPER model[32] is a parametric rainfall model adapted from the operational R-CLIPER model[51]. Both use parametric functions fitted to NASA Tropical Rainfall Measuring Mission satellite data (1998–2000)[52] to produce symmetric rain fields across three TC intensity classes (TS, Cat 1–2, Cat 3–5). R-CLIPER fits only the mean rainfall within each class; P-CLIPER fits the full probability density function by introducing a free parameter, f, representing the departure from the mean. The value of f is calibrated to the study region using observed rainfall and hydrologic response, then sampled from the calibrated range based on the storm class at landfall or nearest coastal approach for each event. P-CLIPER dynamically selects from the three TC intensity class equation sets using the current wind speed and location to compute rainfall intensity for all points 350 km equidistant from the storm center.

Because the study area was expanded to encompass the eastern half of North Carolina and a new hydrologic model was adopted from previous work[19,20], f was re-calibrated using precipitation pattern matching and hydrologic response analysis for 23 storm events impacting the region from 2002–2023 (manuscript in preparation). This yielded storm-class-specific sampling ranges: TS [-15, 45], Cat 1–2 [15, 90], and Cat 3–5 [40, 90]. The Cat 3–5 range was set by informed judgment based on the Cat 1–2 distribution, as no Cat 3–5 storms made landfall within 350 km of the study region during the calibration period. For each synthetic track, f is sampled from a truncated normal distribution (mean at $f = 0$, tails clipped at the calibrated thresholds) and used to compute hourly rainfall rates. These rates serve as input to EF5 and are accumulated along each track to produce total rainfall fields across the study area.

Inland Flooding

Inland flooding is computed using the Ensemble Framework for Flash Flood Forecasting (EF5)[33], which supports multiple water balance models and routing schemes. We employ the Coupled Routing and Excess STorage (CREST) distributed hydrologic model[35] for water balance computation and a kinematic wave scheme for routing excess rainfall through the river network. Stream discharges from CREST are converted to water surface elevations via stage-discharge relationships and used to estimate fluvial inundation extent through the Height Above Nearest Drainage (HAND) method[53]. Pluvial flooding—driven solely by rainfall accumulation over land independent of the river network—is outside the scope of EF5 and is not considered in this study.

The HAND-based inundation computation is performed as a post-processing step outside of EF5. This is necessary because the version of EF5 used at this time applies a single stream channel threshold for both kinematic wave routing and HAND inundation, and the low threshold required for routing prevents the inundation algorithm from correctly flooding smaller features near large channel pixels. To address this, inundation is computed independently across a range of channel threshold values, and the results are combined into a single inundation map by retaining the maximum depth at each pixel. Within the workflow shown in Figure 1, EF5 takes hourly P-CLIPER rainfall as input and produces hourly discharges for the stream network; post-processing then yields the extent, depth, and duration of fluvial inundation for each event. Implementation details of the inland-flood chain—DEM conditioning and channel burning, parameter development, hydrologic calibration, and known problem areas—are documented in the Supplementary Information.

Storm Surge

Storm surge is modeled using the ADvanced CIRCulation (ADCIRC) model that computes water surface elevations and velocities on triangular, finite-element grids[36]. For North Carolina, we employ a previously validated 608,114 node mesh with horizontal resolution ranging from 10 m in estuaries to 10 km offshore, bathymetry from the Coastal Relief Model, and land elevations from previous work[54]. Surface forcing consists of 10-m wind velocities and atmospheric pressure from the GAHM fields described above.

ADCIRC simulations yield time histories of water surface elevation at each model node, from which peak surge heights (maximum elevation above mean sea level) are extracted and translated to inundation depths using the model's land elevations. Validation against high-water marks from Hurricanes Floyd (1999), Isabel (2003), and Florence (2018) shows median errors of 0.3–0.5 m and 90th-percentile errors below 1.0 m[55].

Loss Modeling

Extending a previously-developed approach[22], we translate hazard intensities into building-level monetary damages using vulnerability functions from Hazus 7.0[39]. Hazus provides empirically calibrated and expert-elicited depth–damage and wind–damage functions that map hazard intensity (wind speed and inundation depth) to expected fractional losses for structures and their contents. Each NSI record is matched to the damage function belonging to the closest Hazus archetype based on occupancy and building attributes including single versus multi-family occupancy, roof/wall/foundation type, number of stories, and age. Formally, this process matches each building, b, to a Hazus archetype, θ, assigning to the building a vector of component $\times$ hazard-specific damage functions, $\mathscr{D}^{c,h}_{\theta(b)}[\cdot] \in [0,1]$, where $c = \{\text{Structure, Contents}\}$ indexes aggregate building components. Damage functions are denominated over hazard exposures, x^h, where $h = \{\text{Wind, Surge, Flood}\}$ indexes hazard types—peak terrain-adjusted wind speed (mph), peak coastal surge inundation depth above ground (ft), and peak fluvial flood inundation depth above ground (ft), respectively. The loss sustained by b attributable to hazard h during storm s is calculated as the product of the exposure-driven fractional damage and the value of the affected component, v_b^c:

$$\ell_{b,s}^h = \mathscr{D}_{\theta(b)}^{\text{Structure},h}[x_{b,s}^h]v_b^{\text{Structure}} + \mathscr{D}_{\theta(b)}^{\text{Contents},h}[x_{b,s}^h]v_b^{\text{Contents}} \tag{1}$$

Aggregating these hazard-specific losses across buildings facilitates investigation of compound extremes, in the specific sense of exposures to multiple hazards that are each severe enough to individually cause damage to the buildings in a given location. For example, for census blocks, i, aggregated losses by hazard are

$$L_{i,s}^h = \sum_{b(i)} \ell_{b,s}^h \tag{2}$$

Importantly, the total damage to a building does not generally equal the sum of the damages attributable to each hazard. Individual elements of a building might be damaged by only a subset of multiple hazards to which they are exposed. In such cases the sum of hazard-specific losses in eq. (1) could exceed the value of the structure and its contents, suggesting problems of double counting. Conversely, individual hazards' damage impacts on elements of a building could reinforce one another, resulting in total losses that exceed the sum of hazard-specific damages. In such circumstances the sum of the hazard-specific losses in eq. (1) would underestimate the total loss. The precise manner in which damages combine to give rise to whole-building loss is not well characterized and highly uncertain. We address this issue by combining damages from multiple hazards using a *maximum damage rule*, which estimates the total loss as the maximum of individual hazard losses at the building level. This calculation yields aggregated block-level losses

$$L_{i,s}^{\star} = \sum_{b(i)} \max\left\{\ell_{b,s}^{\text{Wind}}, \ell_{b,s}^{\text{Surge}}, \ell_{b,s}^{\text{Flood}}\right\}. \tag{3}$$

Eq. (3) is conservative, bounding losses to never exceed the total value of the building and its contents, avoids double-counting, and aligns with insurance industry practice. Its limitation is that it does not account for potential interaction effects (e.g., wind-driven water intrusion amplifying surge damage). Accounting for the latter necessitates probabilistic simulation of damage at the level of each building's constituent elements, something that is beyond Hazus' current capability, and is too computationally costly for the present large-scale application[56]. As a sensitivity check on the maximum-damage rule, we apply an alternative aggregation that sums hazard-specific damage ratios at the building-component level, with the sum capped at 1 (i.e., total loss) to prevent damages from exceeding the total value of a building's components:

$$\widetilde{L}_{i,s}^{\star} = \sum_{b(i)} \left[\min\left\{\sum_h \mathscr{D}_{\theta(b)}^{\text{Structure},h}[x_{b,s}^h],\, 1\right\} v_b^{\text{Structure}} + \min\left\{\sum_h \mathscr{D}_{\theta(b)}^{\text{Contents},h}[x_{b,s}^h],\, 1\right\} v_b^{\text{Contents}}\right]. \tag{4}$$

Eqs. (2) and (3) identify compound hazard extremes. Let $\mathscr{Q}[\cdot]$ denote the quantile operator, and define the mapping

$$(i, s(q)) = \arg\min_s \{L_{i,s}^{\star} - \mathscr{Q}[\mathbf{L}_i^{\star}, q]\}$$

which identifies the storm ensemble member whose total loss at location i most closely matches the local q^{th} quantile threshold. We assess whether each location experiences compound hazards at q via the indicator

$$\mathscr{H}_{i,q} = \begin{cases} \text{None} & L_{i,s(q)}^{\text{Wind}} = L_{i,s(q)}^{\text{Surge}} = L_{i,s(q)}^{\text{Flood}} = 0 \\ \text{Wind only} & L_{i,s(q)}^{\text{Wind}} > 0, L_{i,s(q)}^{\text{Surge}} = L_{i,s(q)}^{\text{Flood}} = 0 \\ \text{Surge only} & L_{i,s(q)}^{\text{Surge}} > 0, L_{i,s(q)}^{\text{Wind}} = L_{i,s(q)}^{\text{Flood}} = 0 \\ \text{Flood only} & L_{i,s(q)}^{\text{Flood}} > 0, L_{i,s(q)}^{\text{Wind}} = L_{i,s(q)}^{\text{Surge}} = 0 \\ \text{Wind + Surge} & L_{i,s(q)}^{\text{Wind}} > 0, L_{i,s(q)}^{\text{Surge}} > 0,\ L_{i,s(q)}^{\text{Flood}} = 0 \\ \text{Wind + Flood} & L_{i,s(q)}^{\text{Wind}} > 0, L_{i,s(q)}^{\text{Flood}} > 0, L_{i,s(q)}^{\text{Surge}} = 0 \\ \text{Surge + Flood} & L_{i,s(q)}^{\text{Surge}} > 0, L_{i,s(q)}^{\text{Flood}} > 0, L_{i,s(q)}^{\text{Wind}} = 0 \\ \text{Wind + Surge + Flood} & L_{i,s(q)}^{\text{Wind}} > 0, L_{i,s(q)}^{\text{Surge}} > 0, L_{i,s(q)}^{\text{Flood}} > 0 \end{cases} \tag{5}$$

The result of this calculation is shown in Fig. 5.

Insurance Model

As the final stage of the modeling framework (Figure 1), we estimate insurance prices and market penetration in a competitive market using a multi-region Cournot–Nash game[57], built on the storm scenarios and losses previously described. Rather than grouping zones by geographic adjacency, the model partitions the study region into pricing zones according to expected losses per home, so that each zone represents a subgroup of properties with similar hurricane risk profiles. This risk-based zoning allows insurers to set differentiated prices that reflect the underlying heterogeneity in vulnerability across the region, avoiding the distortions of a uniform premium that would simultaneously overprices coverage in lower-risk areas and under-price it in higher-risk ones.

Based on the 604 hurricane events, we assume that the aggregate probability of hurricane occurrence is approximately 31%, with the occurrence probability distributed uniformly across individual hurricanes. Based on this hurricane probability distribution, we generate 2,000 simulated scenarios, each with a 30-year horizon, using Monte Carlo simulation to evaluate insurance pricing, insolvency probability, and profitability outcomes.

Homeowner demand within each zone is modeled using an exponential constant absolute risk aversion (CARA) utility function[58,59], in which each homeowner purchases insurance when the utility of paying the premium and deductible exceeds the utility of absorbing uninsured losses. The CARA parameter is drawn from a lognormal distribution calibrated to reproduce observed National Flood Insurance Program penetration rates[60], capturing realistic heterogeneity in risk attitudes across the population. On the supply side, each insurer selects zone-level prices to maximize expected profit across hurricane scenarios over a 30-year horizon[58,61], subject to a solvency constraint limiting the annual insolvency rate to 0.2%. Insurer costs encompass both policyholder claims and premiums paid for excess-of-loss catastrophe reinsurance, characterized by an attachment point and maximum payout, which transfers extreme loss exposure to a re-insurer and preserves insurer solvency under catastrophic scenarios. The insurance products are categorized into two types: wind-only insurance and combined wind + flood insurance. The flood coverage in the combined policy indemnifies both fluvial (inland) flooding and coastal storm surge, so a household holding the combined policy is protected against all three perils, whereas a wind-only household bears its surge and flood losses out of pocket. Premiums and deductibles are on an annual basis. The deductible is set at $2,500 per year for the wind-only policy, while for the combined policy, separate deductibles of $2,500 per year apply to wind and flood coverage, respectively.

Because the resulting demand and cost functions are nonlinear and non-convex across zones simultaneously, equilibrium prices cannot be recovered analytically through standard first-order conditions. We therefore apply a binary search heuristic[62] that exploits insurer homogeneity–all firms share identical cost structures and therefore identical best-response functions–so that at equilibrium every insurer satisfies the same volume of demand in each zone. This symmetry means the search need only locate the point where a single insurer's best-response function intersects the equal-demand axis, rather than tracing the full set of best-response curves for all insurers simultaneously. Within each iteration, a Tabu search metaheuristic[63,64] solves the individual insurer's optimization problem, simultaneously identifying the profit-maximizing price vector across all zones and the optimal reinsurance policy parameters given the aggregate demand satisfied by the remaining insurers.

Data Availability

The National Structure Inventory (NSI) is publicly available from the U.S. Army Corps of Engineers at https://www.hec.usace.army.mil/confluence/nsi; Hazus 7.0 damage functions are distributed by FEMA and openly accessible through the Hazus program https://www.fema.gov/flood-maps/products-tools/hazus; Census block boundaries and block-to-block crosswalks are available from NHGIS https://www.nhgis.org/geographic-crosswalks; Synthetic tropical cyclone tracks and simulated hazard fields generated for this study are available from the project's DesignSafe[65] data archive upon request from the corresponding author.

Code Availability

All code used for loss calculation, hazard-inventory matching, and statistical analysis in this study is publicly available at https://github.com/jhe248/compound_hazard_NC. The repository includes scripts for building inventory processing, Hazus damage function application, extensive and intensive margin analysis, insurance output visualization, and figure generation.

Ethnics Declarations

Competing interests. The authors declare no competing interests.

Ethics approval. Not applicable. This study involves no human participants, animal subjects, or personally identifiable data; the building-level analysis relies on the publicly available National Structure Inventory, which contains no individual-level information.

Acknowledgments

We are grateful to researchers in the Coastal Hazards, Economic prosperity and Resilience (CHEER) Hub for insightful conversations and discussions that have contributed to this effort.

Funding

This research was supported by the U.S. National Science Foundation through the Coastal Hazards, Economic prosperity and Resilience (CHEER) Hub (award no. 2209190), and by the NSF URBAN program (award no. DGE 1735087).

Author Information and Contribution

Corresponding author
Correspondence to Jiahang He (jhhe@bu.edu).

Contribution
J.H. and I.S.W.: conceptualization and project administration; J.H.: data curation, formal analysis, validation, and visualization; J.H., J.P., B.B., C.S., B.C., K.D. and R.K.: investigation; J.H., J.P., B.B., C.S., B.C., K.D., R.K., D.L., L.N. and I.S.W.: methodology; J.H., I.S.W., D.L., L.N., J.P., B.B., C.S., B.C., K.D. and R.K.: software implementation; I.S.W. and L.N.: funding acquisition and supervision; J.H., J.P. and I.S.W.: writing – original draft; J.H., J.P., I.S.W., B.B., C.S., B.C., D.L. and L.N.: writing – review & editing.

A. Fraction of Population, Asset Value, and Homes with Nonzero Loss Probability

Hazard Category	Frac. Pop. (%)	Frac. Value (%)	Frac. Homes (%)
Any loss	64.3	65.2	63.0
Wind	64.2	65.1	62.9
Surge	1.2	1.4	1.5
Flood	2.3	2.2	2.2
Wind + Surge	2.0	2.5	2.6
Wind + Flood	3.0	2.8	2.8
Flood + Surge	0.09	0.08	0.08
Wind + Flood + Surge	0.29	0.27	0.29

B. Quantiles of Per-Property Damage Probability (%)

Hazard Category	P50	P95	P99
Any loss	5.3	18.0	19.7
Wind	5.3	16.2	19.0
Surge	0.83	10.8	27.2
Flood	0.66	10.9	95.4
Wind + Surge	1.2	8.1	12.6
Wind + Flood	0.66	4.5	7.5
Flood + Surge	0.17	0.99	3.3
Wind + Flood + Surge	0.33	1.8	3.1

C. Population (thousands) and Asset Exposures ($billions) at Probability Quantiles

	P50		P95		P99	
Hazard Category	Pop. (000)	Val. ($B)	Pop. (000)	Val. ($B)	Pop. (000)	Val. ($B)
Any loss	1,355	314.2	121	35.8	19	7.4
Wind	1,326	306.6	126	34.2	28	8.0
Surge	23	7.2	2	0.8	<1	0.1
Flood	47	11.1	3	1.1	<1	0.2
Wind + Surge	38	12.5	3	1.4	<1	0.3
Wind + Flood	61	13.6	5	1.4	1	0.3
Flood + Surge	4	0.7	<1	0.05	<1	0.01
Wind + Flood + Surge	8	1.9	<1	0.2	<1	0.04

Table 1. Extensive margin characterization of hazard exposure across the 604-storm ensemble. Panel A reports the fraction of homes, population, and asset value that have a nonzero probability of sustaining each type of loss. Panel B reports quantiles (P50, P95, P99) of the per-home damage occurrence probability (fraction of 604 storms producing positive loss), computed over the homes in Panel A with nonzero damage probability. Panel C reports the population (millions) and asset value ($ billions) in homes whose occurrence probability is at or above the corresponding Panel B quantile—the exposure concentrated at or beyond that probability level—so each entry is bounded by the category's exposed total and declines from P50 to P99. Because homes are unevenly distributed across grid cells, the per-home probability quantiles weight each 250-m cell by the number of homes it contains. Quantile thresholds are computed separately for each hazard category, and occurrence probabilities take discrete values (multiples of 1/604), so entries are comparable within rows but need not nest exactly down columns.

	Homes affected (%)	Homes / storm	Mean Loss ($)	Median Loss ($)	P95 Loss ($)	Mean LR (%)	Median LR (%)	P95 LR (%)
Panel A: Single-Hazard Conditional Severity								
Wind	99.99	117,429	54,052	623	217,209	5.1	0.1	39.9
Flood	6.03	3,121	262,049	159,847	845,522	37.0	33.3	68.7
Surge	4.01	2,353	199,830	103,373	667,704	22.8	19.7	49.0
Panel B: Compound-Hazard Conditional Severity								
Wind + Surge	3.82	1,371	294,808	139,300	1,048,226	31.5	24.0	79.8
Wind + Flood	5.75	1,000	275,465	145,356	949,492	35.1	30.7	74.0
Wind + Flood + Surge	0.63	54	338,329	188,669	1,146,166	46.7	44.0	87.4
Flood + Surge	0.16	9	210,999	109,063	854,835	33.1	29.7	64.7

Table 2. Conditional loss severity by hazard type. "Homes affected" is the percentage of the 575,453 RES1 single-family homes that sustain the given category of loss in at least one of the 604 storms; "Homes/storm" is the mean number of homes damaged per storm (total damaged building–storm records divided by 604). Panel A reports building–storm pairs experiencing positive damage from a single hazard type. Panel B reports compound events where damage from two or more hazards co-occur. "LR" denotes loss ratio (loss divided by building replacement value). Across the ensemble, 99.99% of homes sustain any loss and 9.0% experience at least one compound (two-or-more hazard) event.

	Wind-only policy		Wind+Flood policy	
Hazard category	$ (B)	% of value	$ (B)	% of value
Panel A: Individual hazards				
Wind only	17.60	30.87	17.60	30.87
Surge only	0.09	0.16	0.00	0.00
Flood only	0.01	0.01	0.00	0.00
Panel B: Compound hazards				
Wind + Surge	12.66	22.20	10.64	18.66
Wind + Flood	2.62	4.59	2.03	3.56
Surge + Flood	0.01	0.03	0.00	0.00
Wind + Surge + Flood	1.12	1.96	0.59	1.03
Panel C: Aggregates				
Subtotal: individual	17.70	31.04	17.60	30.87
Subtotal: compound	16.41	28.78	13.26	23.25
Total	**34.11**	**59.82**	**30.86**	**54.12**

Table 3. Worst-case uninsured losses by hazard category and insurer-offered policy. For each building, the worst-case storm under each policy is the storm in the 604-storm ensemble that yields the largest uninsured loss given that policy's coverage rules; the loss is then attributed to the hazard category of the driving storm. Dollar values are billions; percentages are shares of total building-plus-contents value across the 196,619-building sample ($57.0 B). Under *Wind-only*, wind uptakers (34.6% of buildings) have wind reimbursed and bear surge + flood out-of-pocket; non-uptakers bear all losses. Under *Wind+Flood*, buildings holding both policies (10.2%) bear nothing, buildings holding wind alone (24.3%) keep their wind coverage and bear surge + flood, and non-purchasers bear all losses. Because every flood-policy holder also holds wind, broadening the offered coverage from wind-only to wind+flood can only reduce uninsured losses. Coverage decisions are those of the affordability-constrained equilibrium.

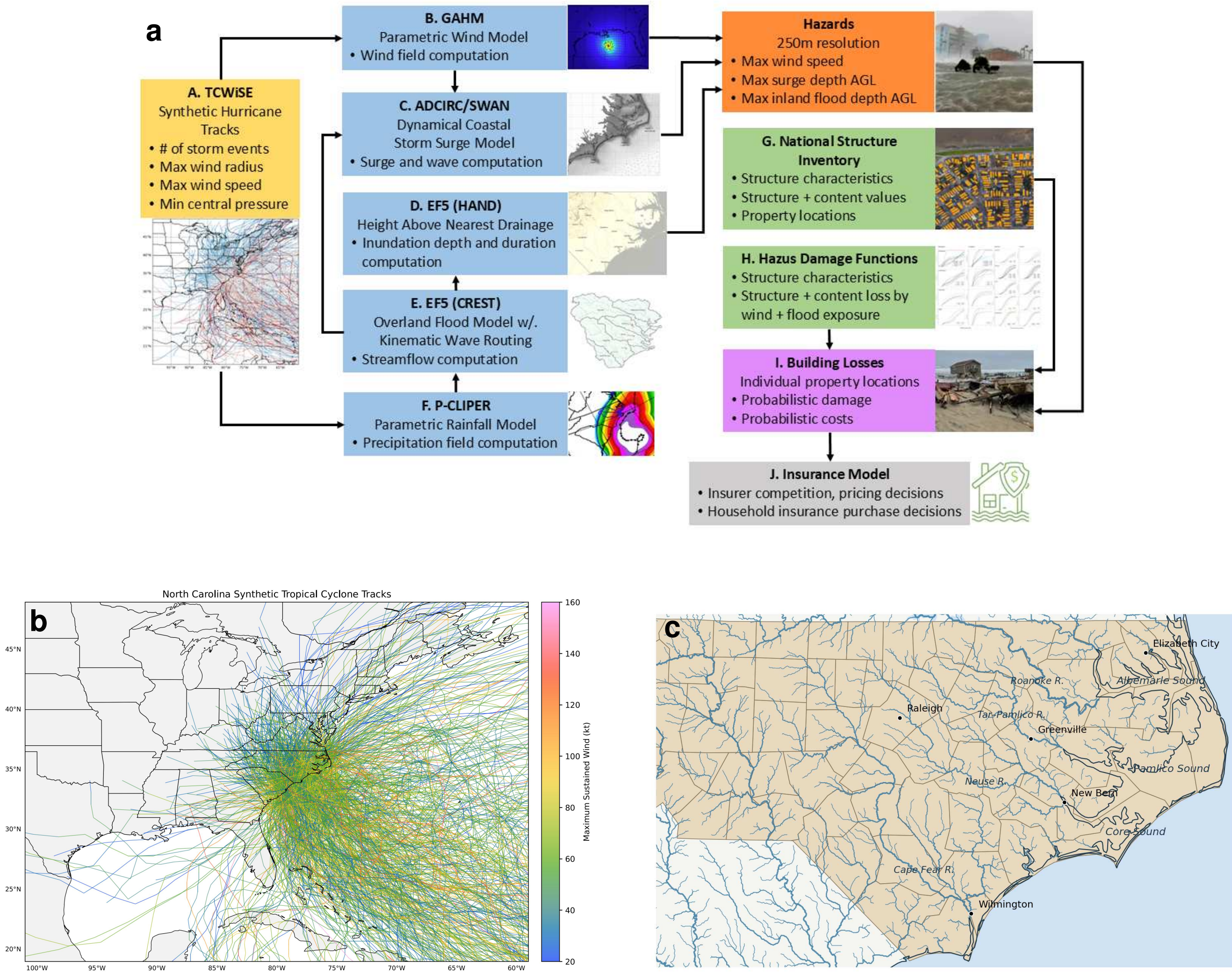

Figure 1. Compound TC hazard modeling framework. (**a**) Workflow integrating the TCWiSE synthetic-track model, GAHM wind, P-CLIPER rainfall, EF5 hydrology, and ADCIRC storm surge. (**b**) Synthetic tropical cyclone tracks across the western North Atlantic, coloured by maximum sustained wind speed (kt; 1 kt $\approx$ 0.514 m s^{-1}). (**c**) Eastern North Carolina study domain: NC counties analysed (tan), drainage network from HydroSHEDS (blue lines), Atlantic coastline and sounds; major rivers and key cities labelled.

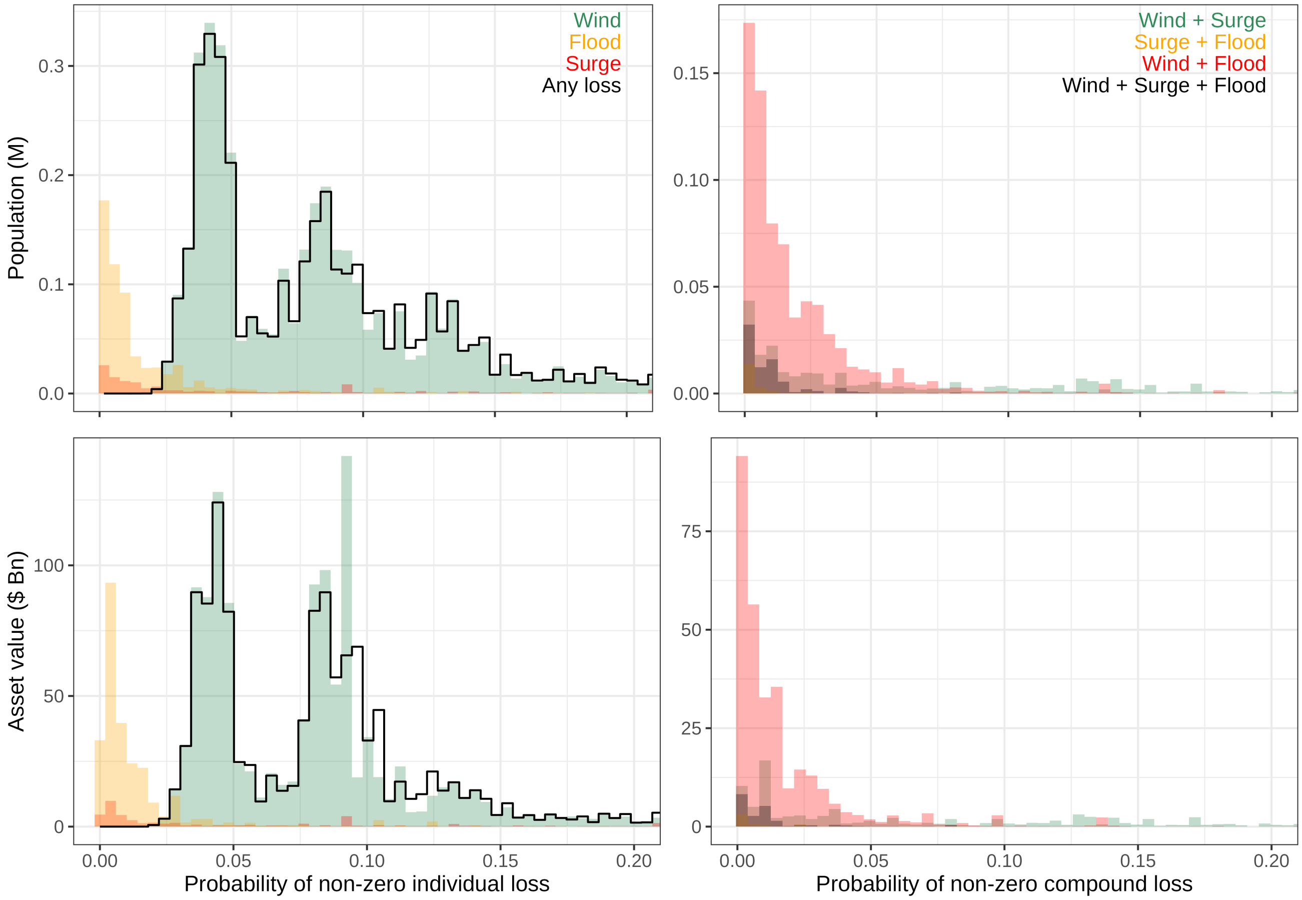

Figure 2. Distributions of exposed population and asset value by the probability of nonzero individual and compound losses. (**a**, **c**) Distributions of (**a**) population (millions) and (**c**) asset value ($ billions) across per-block probabilities of nonzero loss for wind only, surge only, and flood only hazards; the black outline marks the any-loss envelope. (**b**, **d**) Distributions of (**b**) population and (**d**) asset value across per-block probabilities of nonzero loss for wind + surge, wind + flood, surge + flood, and wind + surge + flood hazards.

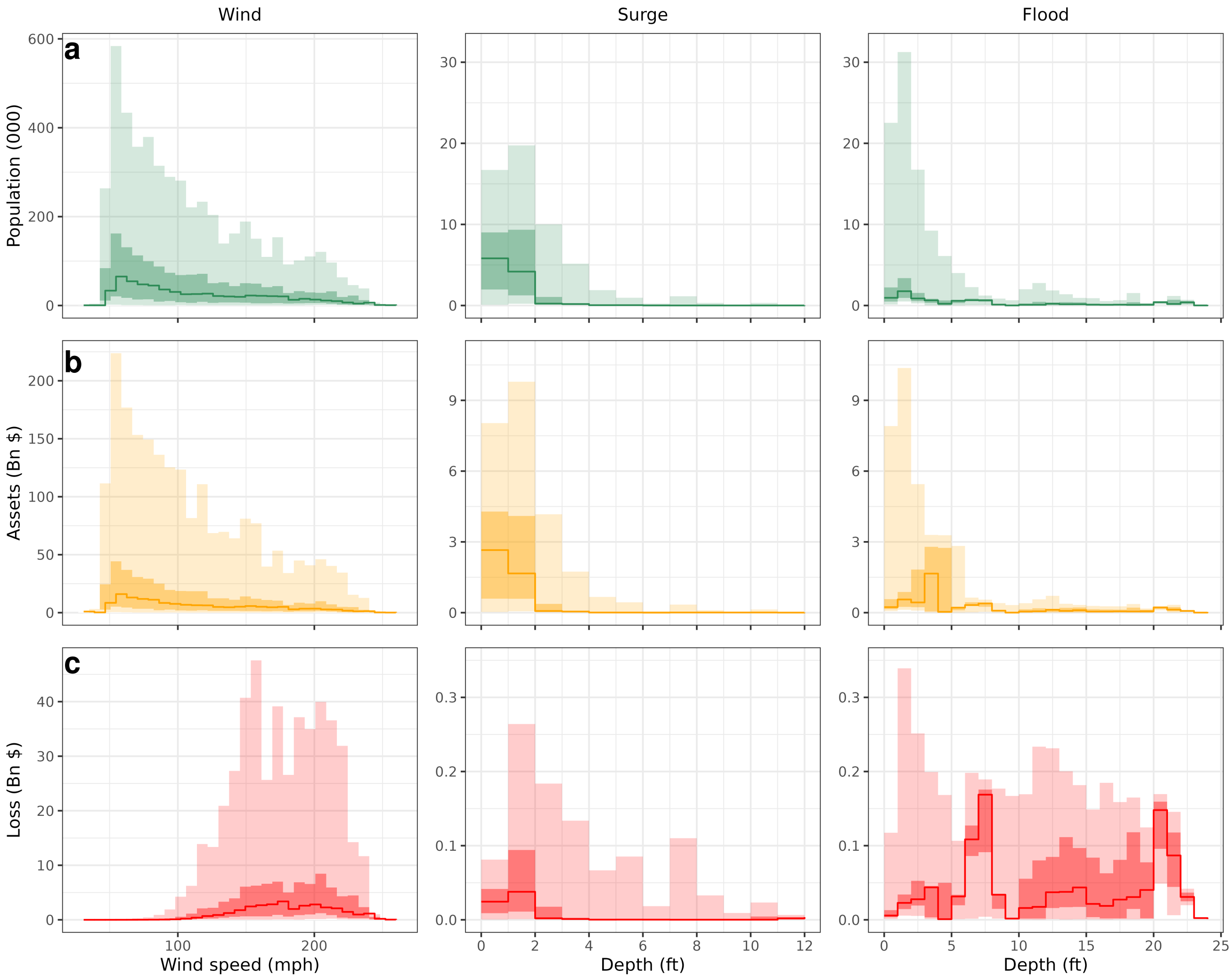

Figure 3. Distributions of (a) population exposure (thousands), (b) asset value exposure ($ billions), and (c) loss ($ billions) by individual hazard intensity. Columns represent wind speed in mph (left), surge depth in ft (center), and flood depth in ft (right). Light shading indicates the 95% confidence interval across the 604-storm ensemble; dark shading indicates the inter-quartile range; the solid line marks the median of the distribution of non-zero losses.

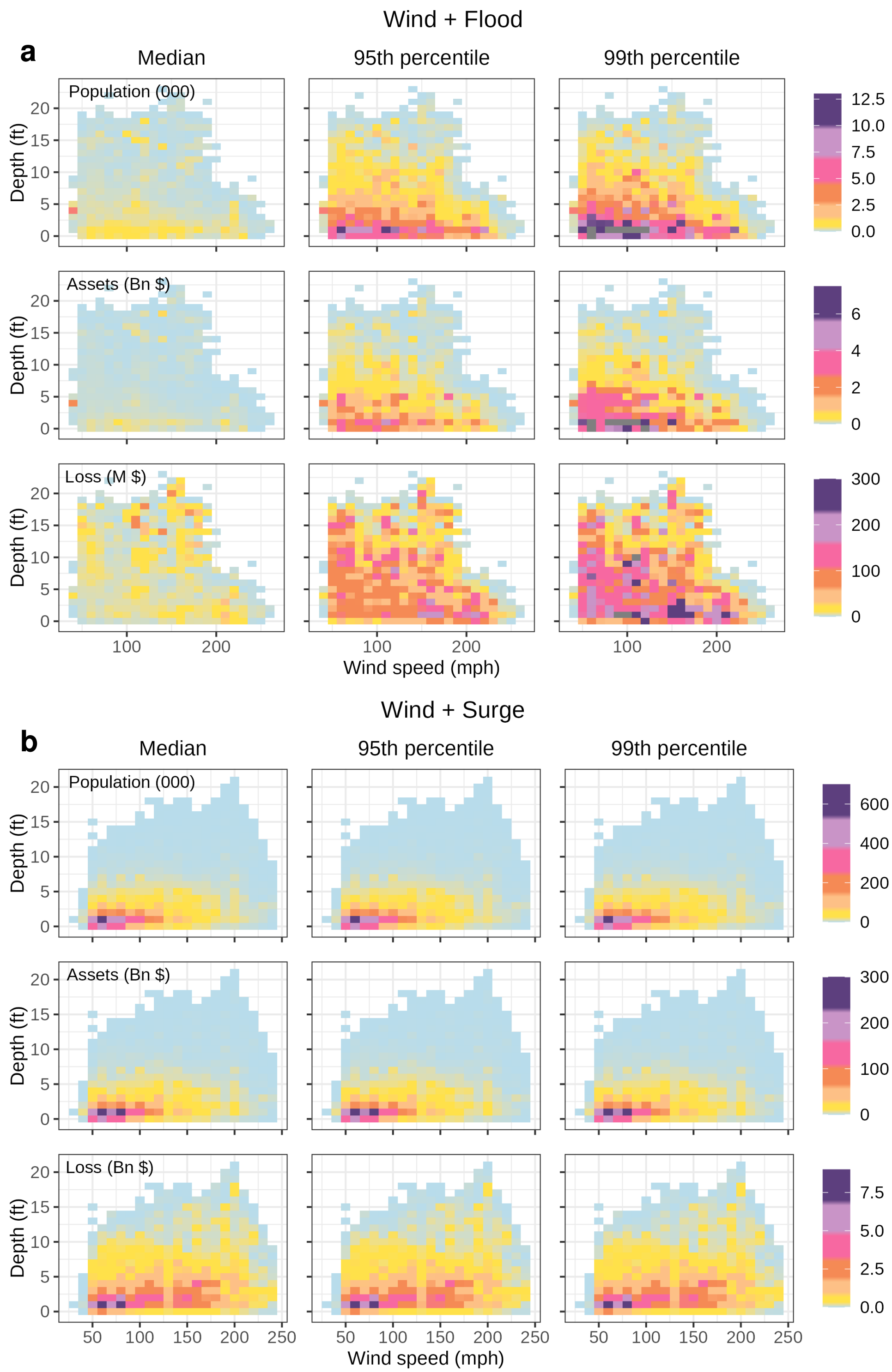

Figure 4. Bivariate distributions of hazard intensity, exposure, and loss for compound (a) wind + flood and (b) wind + surge events. Columns represent the nonzero-loss quantile (median, 95th, and 99th percentile of the distribution of losses over TCs producing positive damage), and rows represent population exposed (top, in thousands), asset value exposed (middle, in billions), and loss (bottom, in billions). Colors indicate the magnitude of exposure or loss at different wind speed and inundation depth intervals.

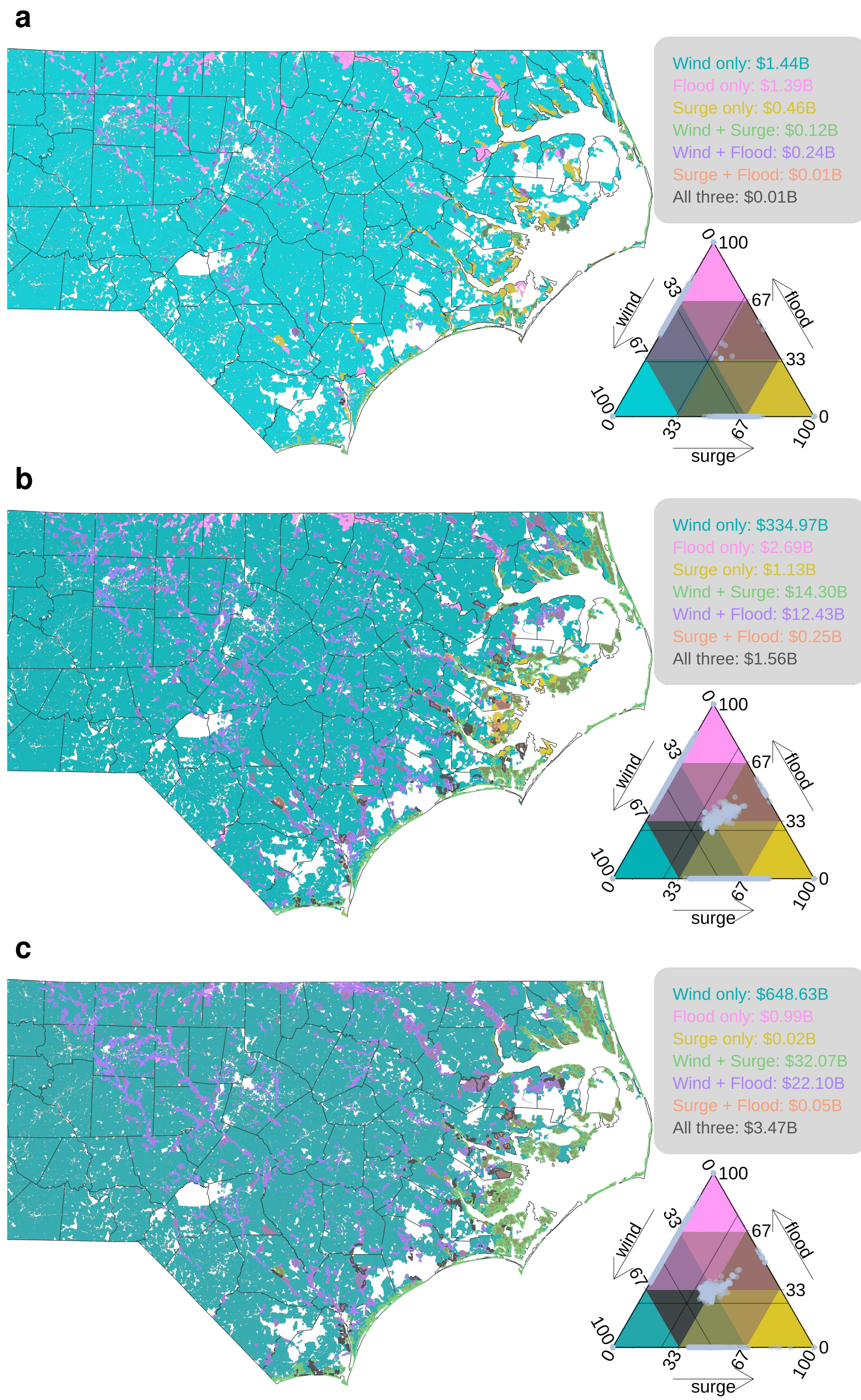

Figure 5. Census block individual and compound losses at quantiles of the distribution of nonzero losses. Each block's loss is computed from the ensemble member whose losses most closely match the block's percentile across all TC events that generate local nonzero losses. Loss proportions are log-transformed to prevent extreme single-hazard events from masking co-occurring hazards. The upper-right legend lists each hazard category's total loss summed across all qualifying blocks in the panel; these are separate per-category totals, not cumulative.

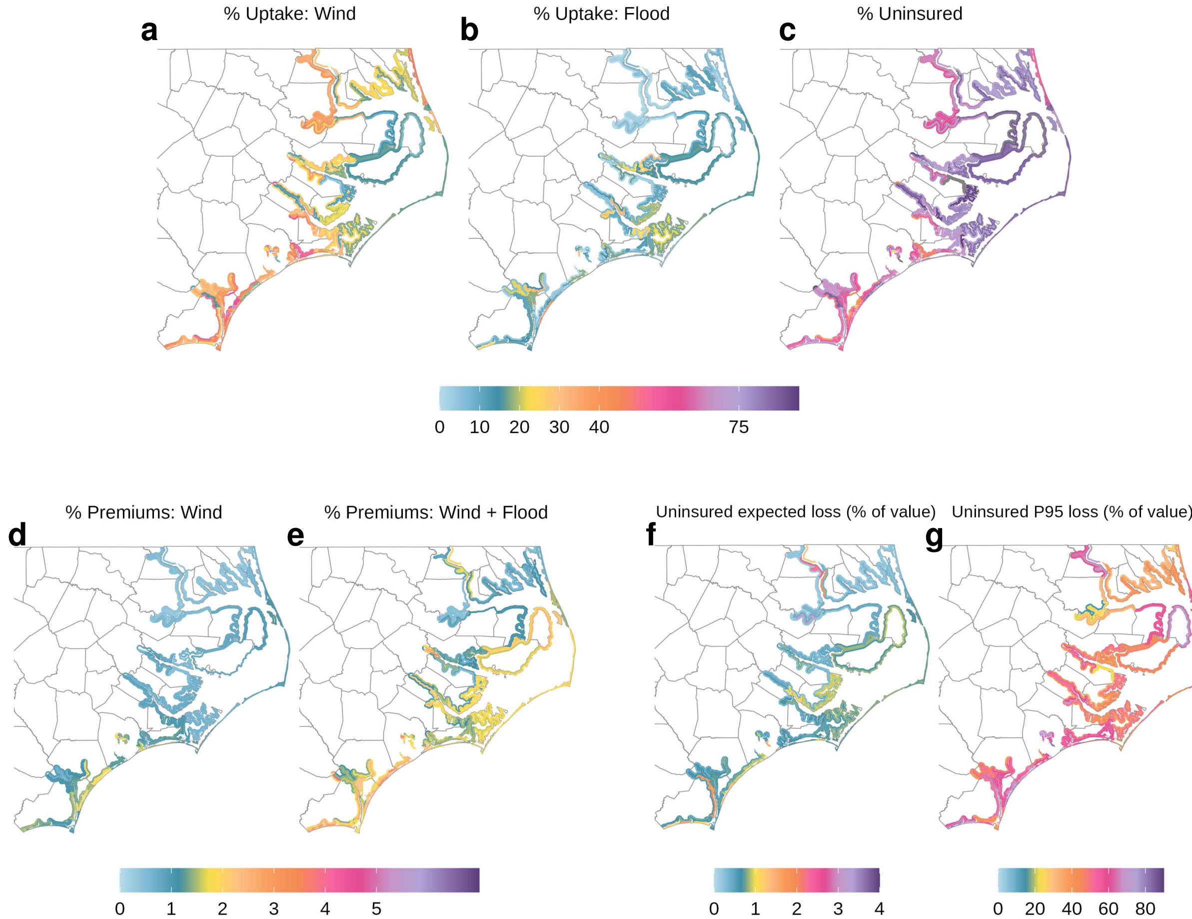

Figure 6. Simulated insurance market outcomes for 196,619 single-family homes across the coastal pricing zones of eastern North Carolina (see Methods). (**a**–**c**) Policy uptake, as a percentage of homes: (**a**) wind coverage, (**b**) flood coverage, and (**c**) the uninsured share. Every flood-policy holder also holds wind, so panel (**b**) is flood-coverage uptake among homes that all carry wind. (**d**, **e**) Equilibrium annual premium as a percentage of building-plus-contents value for the (**d**) wind-only policy and the (**e**) combined wind + flood policy (the combined premium sums the wind and flood premiums). (**f**, **g**) Uninsured loss as a percentage of building-plus-contents value, computed at the zone level as the summed loss over uninsured homes divided by their summed value: (**f**) expected annual loss and (**g**) the 95th-percentile (tail) loss. Panels (**f**) and (**g**) use different colour scales—expected loss reaches only a few percent of value, whereas the 95th-percentile loss is an order of magnitude larger—underscoring how steeply the uninsured loss ratio climbs from the mean to the tail in the compound-exposed coastal zones.

References

1. Zscheischler, J. *et al.* Future climate risk from compound events. *Nature climate change* **8**, 469–477 (2018).
2. Vaidyanathan, A., Kegler, S. R., Saha, S. S. & Mulholland, J. A. A statistical framework to evaluate extreme weather definitions from a health perspective: A demonstration based on extreme heat events. *Bulletin of the American Meteorological Society* **97**, 1817 – 1830, DOI: 10.1175/BAMS-D-15-00181.1 (2016).
3. Keim, B. D., Muller, R. A. & Stone, G. W. Spatiotemporal patterns and return periods of tropical storm and hurricane strikes from texas to maine. *Journal of Climate* **20**, 3498 – 3509, DOI: 10.1175/JCLI4187.1 (2007).
4. Griffin, M., Malsick, M., Mizzell, H. & Moore, L. Historic rainfall and record-breaking flooding from hurricane florence in the pee dee watershed. *Journal of South Carolina Water Resources* **6**, 9 (2019).
5. Reed, K. A., Stansfield, A., Wehner, M. & Zarzycki, C. Forecasted attribution of the human influence on hurricane florence. *Science advances* **6**, eaaw9253 (2020).
6. Grimley, L. E., Hollinger Beatty, K. E., Sebastian, A., Bunya, S. & Lackmann, G. M. Climate change exacerbates compound flooding from recent tropical cyclones. *npj Natural Hazards* **1**, 45 (2024).
7. Gori, A., Lin, N. & Smith, J. Assessing compound flooding from landfalling tropical cyclones on the north carolina coast. *Water Resources Research* **56**, e2019WR026788 (2020).
8. Czajkowski, J., Villarini, G., Michel-Kerjan, E. & Smith, J. A. Determining tropical cyclone inland flooding loss on a large scale through a new flood peak ratio-based methodology. *Environmental Research Letters* **8**, 044056, DOI: 10.1088/1748-9326/8/4/044056 (2013).
9. Pricope, N. G., Hidalgo, C., Pippin, J. S. & Evans, J. M. Shifting landscapes of risk: Quantifying pluvial flood vulnerability beyond the regulated floodplain. *Journal of Environmental Management* **304**, 114221, DOI: 10.1016/j.jenvman.2021.114221 (2022). TLDR: The areal extent of post-Hurricane Florence floodwater within and beyond the 100-year floodplain (SFHA) and the proportion of residential structures exposed to flooding within an eight-county study area are quantified using nearly-coincident high-spatial, high-temporal resolution CubeSat satellite imagery.
10. Garcia, H. M. *et al.* Reconstructing Repetitive Flood Exposure Across 78 Events From 1996 to 2020 in North Carolina, USA. *Earth's Future* **13**, e2025EF006026, DOI: 10.1029/2025EF006026 (2025).
11. Kunkel, K. E. *et al.* Meteorological causes of the secular variations in observed extreme precipitation events for the conterminous united states. *Journal of Hydrometeorology* **13**, 1131–1141 (2012).
12. Lin, N., Emanuel, K., Oppenheimer, M. & Vanmarcke, E. Physically based assessment of hurricane surge threat under climate change. *Nature Climate Change* **2**, 462–467 (2012).
13. Knutson, T. *et al.* Tropical cyclones and climate change assessment: Part ii: Projected response to anthropogenic warming. *Bulletin of the American Meteorological Society* **101**, E303–E322 (2020).
14. Gori, A., Lin, N., Xi, D. & Emanuel, K. Tropical cyclone climatology change greatly exacerbates US extreme rainfall–surge hazard. *Nature Climate Change* **12**, 171–178, DOI: 10.1038/s41558-021-01272-7 (2022).
15. Wing, O. E. *et al.* Inequitable patterns of us flood risk in the anthropocene. *Nature Climate Change* **12**, 156–162 (2022).
16. Tesselaar, M. *et al.* Regional inequalities in flood insurance affordability and uptake under climate change. *Sustainability* **12**, 8734 (2020).
17. Gourevitch, J. D., Snyder, M. & Kousky, C. Effects of risk-based pricing reform on flood insurance uptake. *Journal of Catastrophe Risk and Resilience* **3** (2025).
18. Kousky, C. & Cooke, R. Explaining the failure to insure catastrophic risks. *The Geneva Papers on Risk and Insurance-Issues and Practice* **37**, 206–227 (2012).
19. Dresback, K. M. *et al.* Skill assessment of a real-time forecast system utilizing a coupled hydrologic and coastal hydrodynamic model during hurricane irene (2011). *Continental Shelf Research* **71**, 78–94 (2013).
20. Blanton, B. *et al.* An integrated scenario ensemble-based framework for hurricane evacuation modeling: Part 2—hazard modeling. *Risk Analysis* **40**, 117–133 (2020).
21. Grimley, L. E., Sebastian, A. & Gori, A. Emerging importance of compound flooding in future tropical cyclone hazard profiles. *Earth's Future* **14**, e2025EF007367, DOI: 10.1029/2025EF007367 (2026).
22. Liu, D. *et al.* Unequal economic consequences of coastal hazards: hurricane impacts on north carolina. *Environmental Research Letters* **19**, 104003 (2024).

23. Kunreuther, H. C. & Michel-Kerjan, E. O. *At war with the weather: Managing large-scale risks in a new era of catastrophes* (MIT Press, 2011).

24. Born, P. & Viscusi, W. K. The catastrophic effects of natural disasters on insurance markets. *Journal of risk and Uncertainty* **33**, 55–72 (2006).

25. Mills, E. Insurance in a climate of change. *Science* **309**, 1040–1044 (2005).

26. Roper, J. A., Casagrande, D. G. & Bocchini, P. Climate change and insurance: embracing resilience for private market survival. *Sustainable Development* **33**, 8499–8510 (2025).

27. U.S. Army Corps of Engineers. *National Structure Inventory*. U.S. Army Corps of Engineers (2022). Version 2.0.

28. U.S. Army Corps of Engineers. *National Structure Inventory: Technical Documentation Version 2.0*. U.S. Army Corps of Engineers (2022).

29. Nederhoff, K. *et al.* Simulating synthetic tropical cyclone tracks for statistically reliable wind and pressure estimations. *Natural Hazards and Earth System Sciences Discussions* **2020**, 1–30 (2020).

30. Holland, G. J. An analytic model of the wind and pressure profiles in hurricanes. *Monthly Weather Review* **108**, 1212–1218 (1980).

31. Gao, J. *On the surface wind stress for storm surge modeling*. Ph.D. thesis, The University of North Carolina at Chapel Hill (2018).

32. Geoghegan, K. M., Fitzpatrick, P., Kolar, R. L. & Dresback, K. M. Evaluation of a synthetic rainfall model, P-CLIPER, for use in coastal flood modeling. *Natural Hazards* **92**, 699–726 (2018).

33. Flamig, Z. L., Vergara, H. & Gourley, J. J. The ensemble framework for flash flood forecasting (EF5) v1. 2: Description and case study. *Geoscientific Model Development* **13**, 4943–4958 (2020).

34. Nobre, A. D. *et al.* Height above the nearest drainage–a hydrologically relevant new terrain model. *Journal of Hydrology* **404**, 13–29 (2011).

35. Wang, J. *et al.* The coupled routing and excess storage (CREST) distributed hydrological model. *Hydrological sciences journal* **56**, 84–98 (2011).

36. Luettich Jr, R. A., Westerink, J. J. & Scheffner, N. W. ADCIRC: An Advanced Three-Dimensional Circulation Model for Shelves, Coasts, and Estuaries. Report 1. Theory and Methodology of ADCIRC-2DDI and ADCIRC-3DL. Tech. Rep., Coastal Engineering Research Center, U.S. Army Engineer Waterways Experiment Station (1992).

37. Westerink, J. *et al.* A basin- to channel-scale unstructured grid hurricane storm surge model applied to Southern Louisiana. *Mon. Weather Rev.* **136**, 833–864 (2008).

38. Dietrich, J. *et al.* Hurricane Gustav (2008) waves and storm surge: hindcast, synoptic analysis, and validation in Southern Louisiana. *Monthly Weather Review* **139**, 2488–2522 (2011).

39. FEMA. *Hazus Hurricane Model Technical Manual, Hazus 7.0*. Federal Emergency Management Agency, Washington, DC (2024).

40. Howell, J. & Elliott, J. R. Damages Done: The Longitudinal Impacts of Natural Hazards on Wealth Inequality in the United States. *Social Problems* **66**, 448–467, DOI: 10.1093/socpro/spy016 (2019).

41. Ali, J. *et al.* Multivariate compound events drive historical floods and associated losses along the U.S. East and Gulf coasts. *npj Natural Hazards* **2**, 19, DOI: 10.1038/s44304-025-00076-5 (2025).

42. Manson, S., Schroeder, J., Van Riper, D., Kugler, T. & Ruggles, S. IPUMS National Historical Geographic Information System: Version 18.0, DOI: 10.18128/D050.V18.0 (2023).

43. Gahtan, J. *et al.* International Best Track Archive for Climate Stewardship (IBTrACS) Project, Version 4.01. Tech. Rep., NOAA National Centers for Environmental Information (2024).

44. Knapp, K. R., Kruk, M. C., Levinson, D. H., Diamond, H. J. & Neumann, C. J. The international best track archive for climate stewardship (IBTrACS) unifying tropical cyclone data. *Bulletin of the American Meteorological Society* **91**, 363–376 (2010).

45. Landsea, C. W., Harper, B. A., Hoarau, K. & Knaff, J. A. Can we detect trends in extreme tropical cyclones? *Science* **313**, 452–454 (2006).

46. Huang, B. *et al.* Improvements of the daily optimum interpolation sea surface temperature (DOISST) version 2.1. *Journal of Climate* **34**, 2923–2939 (2021).

47. Romero, D. *et al.* Assessment of synthetic tropical cyclones in the north atlantic basin. *Atmospheric Research* 108404 (2025).

48. Kaplan, J. & DeMaria, M. A simple empirical model for predicting the decay of tropical cyclone winds after landfall. *Journal of Applied Meteorology and Climatology* **34**, 2499–2512 (1995).

49. Phillipson, L. & Toumi, R. A physical interpretation of recent tropical cyclone post-landfall decay. *Geophysical Research Letters* **48**, e2021GL094105 (2021).

50. Holland, G. J., Belanger, J. I. & Fritz, A. A revised model for radial profiles of hurricane winds. *Monthly Weather Review* **138**, 4393–4401 (2010).

51. Marks Jr, F. D. Development of a tropical cyclone rainfall climatology and persistence (R-CLIPER) model. Tech. Rep., NOAA/OAR/AOML/Hurricane Research Division (2003).

52. Lonfat, M., Marks Jr, F. D. & Chen, S. S. Precipitation distribution in tropical cyclones using the Tropical Rainfall Measuring Mission (TRMM) Microwave Imager: A global perspective. *Monthly Weather Review* **132**, 1645–1660 (2004).

53. Rennó, C. D. *et al.* Hand, a new terrain descriptor using srtm-dem: Mapping terra-firme rainforest environments in amazonia. *Remote Sensing of Environment* **112**, 3469–3481 (2008).

54. Blanton, B. *et al.* Report for the state of north carolina floodplain mapping project: Coastal flood analysis system. Tech. Rep. TR-08-08, Renaissance Computing Institute, The University of North Carolina at Chapel Hill (2008).

55. Blanton, B. & Luettich, R. North Carolina Floodplain Mapping Program: Coastal Flood Insurance Study - Water Level Validation Study. Technical Report TR-10-06, Renaissance Computing Institute, The University of North Carolina at Chapel Hill (2010).

56. Nofal, O. M. *et al.* Methodology for regional multihazard hurricane damage and risk assessment. *Journal of Structural Engineering* **147**, 04021185 (2021).

57. Liu, D. *et al.* Computing multi-region competitive prices for hurricane-related insurance. *International Journal of Disaster Risk Reduction* **120**, 105383 (2025).

58. Gao, Y., Nozick, L., Kruse, J. & Davidson, R. Modeling competition in a market for natural catastrophe insurance. *Journal of Insurance Issues* 38–68 (2016).

59. Kesete, Y. *et al.* Modeling insurer-homeowner interactions in managing natural disaster risk. *Risk analysis* **34**, 1040–1055 (2014).

60. Dixon, L., Clancy, N., Seabury, S. A. & Overton, A. The national flood insurance program's market penetration rate: Estimates and policy implications. *Santa Monica, CA: RAND Corporation* (2006).

61. Guo, C. *et al.* Dynamic modeling of public and private decision-making for hurricane risk management including insurance, acquisition, and mitigation policy. *Risk Management and Insurance Review* **25**, 173–199 (2022).

62. Brady, M., Mamanduru, V. K. & Tiwari, M. K. An evolutionary algorithmic approach to determine the nash equilibrium in a duopoly with nonlinearities and constraints. *Expert systems with applications* **74**, 29–40 (2017).

63. Glover, F. Tabu search—part i. *ORSA Journal on computing* **1**, 190–206 (1989).

64. Glover, F. Tabu search—part ii. *ORSA Journal on computing* **2**, 4–32 (1990).

65. Rathje, E. M. *et al.* DesignSafe: New cyberinfrastructure for natural hazards engineering. *Natural Hazards Review* **18**, 06017001 (2017).